# Dynamics Analysis and Control of a Holonomic Vehicle With a Continuously Variable Transmission

**Karim A. Tahboub**
College of Engineering and Technology,
Palestine Polytechnic University,
Hebron, Palestine
e-mail: tahboub@ppu.edu

**Harry H. Asada**
Department of Mechanical Engineering,
Massachusetts Institute of Technology,
Cambridge, MA 02139
e-mail: asada@mit.edu

*This paper presents kinematic and dynamic analysis of a holonomic vehicle with continuously-variable transmission. Four ball wheels, independently actuated by DC motors, enable for moving the vehicle in any direction within the plane and rotating it around its center. The angle between the two beams holding the balls can be changed to alter the gear ratio and other dynamic characteristics of the vehicle. This feature is exploited in augmenting the vehicle stability, optimizing output power, selecting an appropriate gear ratio, and in impedance matching. A simple adaptive friction-compensation-based controller is proposed to handle the complex friction properties.* [DOI: 10.1115/1.1434270]

## 1 Introduction

Automobile engines are usually accompanied by gearboxes to satisfy varying torque-speed requirements. In contrast to that, electromechanical drives have, in general, fixed gearing.

Accordingly and as the torque-speed requirements vary, the efficiency of such drives degrades. Since most mobile robots, which are actuated mainly by electromechanical drives, have onboard power supplies (batteries), power efficiency becomes a crucial factor in the applicability of such vehicles. Hence, the necessity of using variable transmission with electromechanical drives becomes clear. Unfortunately, the bulkiness and momentary interruption in power transmission while changing ratios made stepped variable transmission mechanisms unfavorable.

The pursuit of continuously variable transmission (CVT) began as early as 1897, when Maugras invented his split-torque version [1]. Only recent advancements in tribology, material science, and electronic control have made CVT's a very interesting proposition. The automobile industry was encouraged to use CVT's to increase fuel efficiency of the engine [2].

On the other hand, CVT technology is emerging for electromechanical drives. Examples include ball and disk CVT's, cone drives, variable pitch V-belts, and X-screw drives [3].

In the robotics literature, a large number of wheeled or tracked platform mechanisms have been studied and developed to provide the holonomity of the vehicle. This includes the Swedish wheel, the omni-alpha wheel, the crawler mechanism, and the orthogonal wheel mechanism [4].

In this paper, a new type of continuously variable transmission developed by the authors' group for holonomic vehicles will be analyzed with regard to kinematic and dynamic behavior and power efficiency. Four ball wheels, independently actuated by DC motors, enable moving the vehicle in any direction within the plane and rotating it around its center. The angle between the two beams holding the balls can be changed to continuously varying the gear ratio. In contrast to any other design, the CVT is imbedded in the design concept, i.e., there is no separate physical entity called the CVT mechanism. This makes this design more attractive, especially regarding the weight of the vehicle and the reliability of the system. This new CVT exhibits unique characteristics and superb performance. Complexity of the mechanism, however, creates complex frictional properties, which not only reduce transmission efficiency but also degrade control performance. In the latter half of this paper, an efficient compensation method is applied to the vehicle with CVT.

In Section 2, the principle and mechanism of the CVT is described, this includes the kinematics of the motor-ball mechanism and the relationship between individual ball velocities and generalized vehicle velocities. Section 3 gives the dynamics of the vehicle including different friction forces acting on the system. Power issues related to the novel CVT design are analyzed in Section 4. Section 5 presents the adaptive friction-compensation control. Some simulation experiments including the parameter identification of a prototype and the implementation of the control method are given in Section 6.

## 2 Vehicle Mechanism With Continuously Variable Transmission

**2.1 Mechanism.** In contrast to nonholonomic vehicles, a holonomic vehicle can move in an arbitrary direction continually without changing the direction of the wheels. It can move back and forth, slide sideways, and rotate in place. The novel design [5] is based on a spherical tire mechanism where a solid ball is held by a ring roller mechanism. Power is transmitted from a DC motor through a reduction gear, that is meshed with a ring, to the ball via friction between the ball and the rollers mounted on the ring as shown in Fig 1. This power is responsible for rotating the ball around the $\alpha$-axis to induce the active motion of the ball. The upper rollers allow the ball to rotate freely about the $\beta$-axis and thus the ball will not resist a passive motion resulting from the motion of other balls. Four ball units are mounted on the tips of two intersecting beams as shown in Fig. 2.

Recalling that a nonconstrained vehicle in the plane has three degrees of freedom, it suffices to have three independently-actuated ball mechanisms to achieve any desired motion. However, the extra degree of freedom gained by the fourth ball mechanism is employed in changing the angle between the intersecting beams. This feature allows for reconfiguring the base between narrow and wide footprints to fit better in narrow pathways and to augment static stability (prevent tip over situations). Moreover, this leads to changing continuously the ratio between the actuator speed and the resultant vehicle speed as will be shown in the kinematics section. Therefore, this continuously variable transmission vehicle is able to meet diverse speed and torque requirements and exhibit enhanced maneuverability and efficiency. It will be

Contributed by the Dynamic Systems and Control Division for publication in the JOURNAL OF DYNAMIC SYSTEMS, MEASUREMENT, AND CONTROL. Manuscript received by the Dynamic Systems and Control Division October 6, 2000. Associate Editor: Y. Hurmuzlu.

  

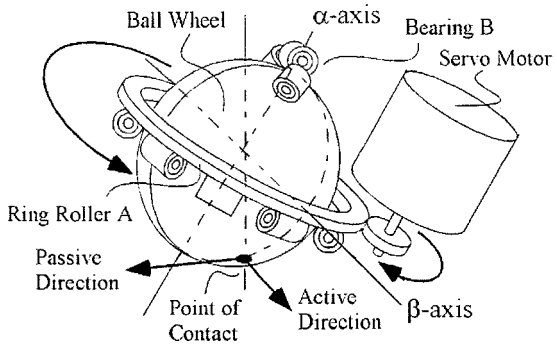


**Fig. 1 Ball wheel unit**

shown, as well, that this characteristic can be utilized in optimizing the power transmitted to the vehicle as well as to match the motors and vehicle impedances.

**2.2 Kinematics.** The effective part of the vehicle (i.e., the chair in the case of a wheelchair application) is mounted on the top of the pivotal joint. For ergonomic reasons, it is required to keep this part (the chair for example) always aligned with the bisector of the two beams (intersecting at the joint) although the two beams rotate about this joint. This calls for using a differential gear mechanism. As shown in Fig. 3, bevel gear 1 is fixed to beam A, bevel gear 2 to beam B, and the chair is mounted on shaft $\alpha$ (which holds shaft $\beta$ that supports bevel gear 3). Accordingly, the angular velocity of the vehicle $\omega_C$, is given by

$$\omega_C = \frac{\omega_A + \omega_B}{2}, \tag{1}$$

where $\omega_A$ and $\omega_B$ are the angular velocities of beam *A* and beam *B*, respectively, all measured about a vertical axis. Thus, it is assured that the chair is kept aligned with the bisector irrespective of the beam motions.

Considering Fig. 3 and Fig. 4, the translational velocity of a ball $v_i$ given the angular speed of the corresponding motor $\omega_i$, and assuming no slippage between the ring rollers and the ball nor between the ball and the ground, is

$$v_i = R\sin(\alpha)\omega_i/\rho, \tag{2}$$

where $\rho$ is the gear reduction ratio, $R$ is the ball radius, and $\alpha = 30$ deg is the inclination angle of the ring. Now, considering only one part of Fig. 4, say the one containing ball *a*, and resolving the velocity of the ball into two components, one obtains

$$\begin{aligned} V_{ix} &= V_{vx} + L(\dot{\phi}_v + \dot{\phi})\cos(\phi) \\ V_{iy} &= V_{vy} + L(\dot{\phi}_v + \dot{\phi})\sin(\phi) \end{aligned} \tag{3}$$

where $V_{ix}$ and $V_{iy}$ are the *x* and *y* velocity components of the *i*th ball, $V_{vx}$ and $V_{vy}$ are the *x* and *y* velocity components of the vehicle ($V_{ix}$, $V_{iy}$, $V_{vx}$, and $V_{vy}$ are all relative to $Xv$ and $Yv$), $L$ is the distance between the pivotal joint to the ball-contact point

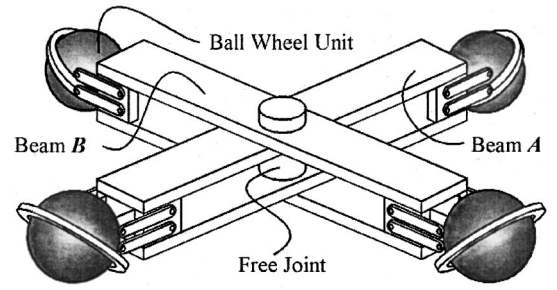


**Fig. 2 Omnidirectional reconfigurable base**

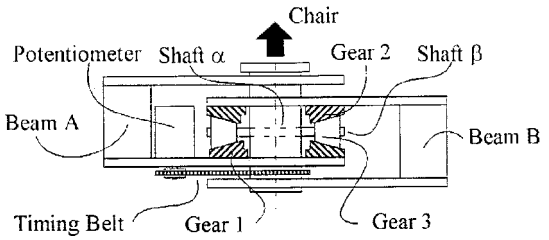


**Fig. 3 Pivotal joint of the vehicle**

with the ground, $\phi$ (later called *base angle*) is half of the angle between the beams, and $\phi_v$ is the angle between the bisector of the beams and a stationary Cartesian *x*-axis i.e., the orientation of the vehicle. Rewriting this equation for the four balls, the following equation can be obtained

$$\begin{bmatrix} V_a \\ V_b \\ V_c \\ V_d \end{bmatrix} = \begin{bmatrix} -\sin\phi & \cos\phi & L & L \\ -\sin\phi & -\cos\phi & L & -L \\ \sin\phi & -\cos\phi & L & L \\ \sin\phi & \cos\phi & L & -L \end{bmatrix} \begin{bmatrix} V_{vx} \\ V_{vy} \\ \dot{\phi}_v \\ \dot{\phi} \end{bmatrix} \tag{4}$$

or in a more compact form $\mathbf{V_i} = J^{-1}\mathbf{V_v}$ (5)

where $J$ is the Jacobian relating the vector of individual velocities $\mathbf{V_i}$ to the vector of generalized velocities $\mathbf{V_v}$. Notice that this Jacobian has a full rank for all possible values of $\phi \in [27.5 \text{ deg}, 62.5 \text{ deg}]$, which means that it is always possible to find a combination of individual ball velocities to generate a desired generalized vehicle velocity.

As stated previously in the Introduction, the novel ball mechanism design allows for a passive motion of the ball. In other words, a certain translational motion of the vehicle may cause a ball to move in a direction other than that perpendicular to the beam. Considering Fig. 4 and following the same derivation as for active velocities, the following relationship for individual ball passive velocities and vehicle generalized velocities is obtained

$$\begin{bmatrix} V_{ap} \\ V_{bp} \\ V_{cp} \\ V_{dp} \end{bmatrix} = \begin{bmatrix} \cos\phi & \sin\phi & 0 & 0 \\ -\cos\phi & \sin\phi & 0 & 0 \\ -\cos\phi & -\sin\phi & 0 & 0 \\ \cos\phi & -\sin\phi & 0 & 0 \end{bmatrix} \begin{bmatrix} V_{vx} \\ V_{vy} \\ \dot{\phi}_v \\ \dot{\phi} \end{bmatrix} \tag{6}$$

or in a more compact form

$$\mathbf{V_{ip}} = P\mathbf{V_v} \tag{7}$$

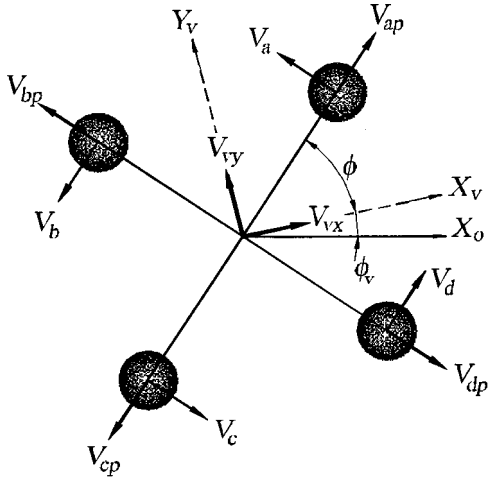


**Fig. 4 Passive and active velocities of balls**

where the subscript $p$ stands for passive. Notice here that neither the rotation of the vehicle nor changing the footprint configuration causes a passive velocity.

Before moving to the dynamics analysis, let us assume a pure translational motion of the vehicle in the $x$-direction, that is $V_{vy} = \dot{\phi}_v = \dot{\phi} = 0$. Thus from Eq. (4), one obtains

$$\begin{bmatrix} V_a \\ V_b \\ V_c \\ V_d \end{bmatrix} = \begin{bmatrix} -\sin\phi \\ -\sin\phi \\ \sin\phi \\ \sin\phi \end{bmatrix} V_{vx}. \tag{8}$$

It is clear, then, that changing the angle $\phi$ would change the ratio of ball velocities to the generalized velocity and thus the "gear" ratio. Hence, this vehicle demonstrates a continuously variable transmission (CVT) feature that can be exploited in different ways as will be discussed in the following sections.

## 3 Dynamics

In this section, the relationship between different forces acting on the vehicle and the resulting vehicle motion will be studied. As the novel vehicle design depends on the deployment of ball wheels, it becomes essential to analyze friction, traction, and twisting forces. Afterwards, a complete dynamics equation will be derived.

**3.1 Friction Analysis.** When a vehicle ball wheel is rotated by the ring roller (see Fig. 1), and because of the inclination of the ring, a tangential *traction force* in the active direction is generated at the point of contact. The magnitude of the traction force cannot exceed the available friction force at the point of contact. Thus, if the applied torque on the ball by the ring roller yields a traction force greater than the available friction a slip will happen and nonholonomicity will occur. To avoid this difficulty, it is assumed throughout this article that enough friction is available to avoid slip. The set of traction forces is responsible for moving the vehicle. However, and as explained in the kinematics section, a ball is allowed to roll freely about the $\beta$-axis (the upper rollers serve this purpose) and thus a ball will not resist a passive motion resulting from the motion of other balls. During such a passive motion, each ball faces a *Coulomb friction force* proportional to the load on it and opposite to the sense of its passive motion. Finally, and for rolling the ball in the presence of friction, it is required to account for an extra torque called the *twisting torque*. These three forces, namely, traction force, friction force, and twisting torque play an important role in the vehicle dynamics. The motion control design relies on a good understanding of these forces as will be highlighted in the control section.

*3.1.1 Twisting Torque.* The ball wheel deforms when a load is applied, hence an area of contact, not a point contact, is created. Hence, when rotating the ball, a resisting torque arises. It is called twisting torque and its magnitude depends on the ball load, the contact area, and the ball and the ground material characteristics.

Twisting torque together with other motor and gear friction torques are lumped to the side of the motor as

$$Tw_i = -\operatorname{sgn}(v_i) f_{ti}/\rho \tag{9}$$

where $f_{ti}$ is its magnitude measured about the $\alpha$-axis of Fig. 1.

*3.1.2 Coulomb Friction.* When a ball translates along a passive motion direction, it overcomes a Coulomb friction force $f_{ip}$, proportional to the load on that ball $W_i$, such that

$$f_{ip} = -\operatorname{sgn}(v_{ip}) \mu_p W_i, \tag{10}$$

where $\mu_p$ is the Coulomb coefficient of friction. The effect of the individual ball Coulomb friction forces on the generalized vehicle forces can be found by means of Eq. (6) to be

$$\begin{bmatrix} F_{px} \\ F_{py} \\ M_{p\phi_v} \\ M_{p\phi} \end{bmatrix} = \begin{bmatrix} c & -c & -c & c \\ s & s & -s & -s \\ 0 & 0 & 0 & 0 \\ 0 & 0 & 0 & 0 \end{bmatrix} \times \begin{bmatrix} \operatorname{sgn}(v_{ap}) & 0 & 0 & 0 \\ 0 & \operatorname{sgn}(v_{bp}) & 0 & 0 \\ 0 & 0 & \operatorname{sgn}(v_{cp}) & 0 \\ 0 & 0 & 0 & \operatorname{sgn}(v_{dp}) \end{bmatrix} \times \begin{bmatrix} f_{ap} \\ f_{bp} \\ f_{cp} \\ f_{dp} \end{bmatrix}, \tag{11}$$

where $c$ and $s$ stand for $\cos\phi$ and $\sin\phi$, respectively. Notice that, since these forces are acting along the beams, they do not cause any vehicle moment. In any case, the traction forces are responsible for overcoming these friction forces together with the inertia of the vehicle and other forces as will be seen in the dynamics equation.

*3.1.3 Traction Forces.* In the same way, the set of ball traction forces can be projected onto the vehicle generalized coordinates (those corresponding to the generalized velocities) by using the duality principle to be

$$\mathbf{F_v} = J^{-T} \mathbf{F_i}, \tag{12}$$

where $\mathbf{F_v} = \lfloor F_x \; F_y \; M_{\phi v} \; M_{\phi} \rfloor$ is the vector containing the four generalized forces corresponding to translation in $x$ and $y$ directions, vehicle rotation, and footprint configuration change, while $\mathbf{F_i}$ contains the four individual traction forces.

**3.2 Dynamics Equation.** The motors are driven by electronic control circuits that regulate the currents supplied to the motors to be proportional to the commanded voltages (output of D/A converter). When compared to the mechanical part of the dynamics, the dynamics of the regulation circuits and that of the armature circuits are fast and thus will be neglected. Accordingly, the torque $T_i$ generated by motor $i$ is

$$T_i(t) = k u_i(t), \tag{13}$$

where $k$ is the result of multiplying the motor torque constant with the voltage/current proportionality constant of the regulating circuit, and $u_i(t)$ is the voltage input to the motor.

Now, by examining the free body diagram given in Fig. 5, this torque has to overcome the motor and ball mechanism inertias and damping, twisting torque, and the traction force. Accordingly

$$T_i(t) = I_m \dot{\omega}_i + d_m \omega_i + R \sin(\alpha) f_i/\rho + \operatorname{sgn}(v_i) f_{ti}/\rho, \tag{14}$$

where $I_m$ is the combined inertia of the motor and the ball, and $d_m$ is the combined damping of the motor and ball. Substituting Eq. (2) and Eq. (13) into Eq. (14), one obtains the following traction-voltage relationship

$$k u_i(t) = (2 I_m \rho/R) \dot{v}_i + (2 d_m \rho/R) v_i + (R/2\rho) f_i + \operatorname{sgn}(v_i) f_{ti}/\rho. \tag{15}$$

The four equations corresponding to the four motors can be put together, and the individual ball velocities and traction forces can be replaced with the generalized vehicle velocities and forces to obtain the dynamic equation. First, putting aside the Coulomb and twisting torques, the relationship between the generalized forces and the generalized accelerations and velocities of the vehicle is found to be

$$\begin{bmatrix} Fx \\ Fy \\ M_{\phi_v} \\ M_{\phi} \end{bmatrix} = \begin{bmatrix} M_v & 0 & 0 & 0 \\ 0 & M_v & 0 & 0 \\ 0 & 0 & I_A+I_B+I_C & I_A-I_B \\ 0 & 0 & I_A-I_B & I_A+I_B \end{bmatrix} \begin{bmatrix} \dot{V}_{vx} \\ \dot{V}_{vy} \\ \ddot{\phi}_v \\ \ddot{\phi} \end{bmatrix} + \begin{bmatrix} Dx & 0 & 0 & 0 \\ 0 & Dy & 0 & 0 \\ 0 & 0 & D\phi_v & 0 \\ 0 & 0 & 0 & D_{\phi} \end{bmatrix} \begin{bmatrix} V_{vx} \\ V_{vy} \\ \dot{\phi}_v \\ \dot{\phi} \end{bmatrix} + \begin{bmatrix} \cos(\phi_v) \\ -\sin(\phi_v) \\ 0 \\ 0 \end{bmatrix} \sin(\theta) M_v g \tag{16}$$

where $M_v$ is the mass of the whole vehicle, $I_A$, $I_B$, and $I_C$ are the inertias of beam *A*, beam *B*, and the vehicle, respectively. All damping forces, as those acting on the motors and the balls together with other unmodelled viscous-like friction forces, are lumped in the second term of the equation. There, and for simplicity only, a diagonal matrix is assumed. $D_x$, for example, denotes vehicle damping coefficient in the *x*-direction. Finally, $M_v g$ is the weight of the vehicle, and $\theta$ is the inclination angle of the plane containing $X_v$ and $Y_v$ from the horizontal (see Fig. 4). Notice that deriving this equation following Newton-Euler requires analyzing the differential gear dynamics (internal reaction forces) as it relates the beams' motions to the vehicle's motion as given by Eq. (1), whereas it suffices to consider only the external forces in the Lagrangian formulation.

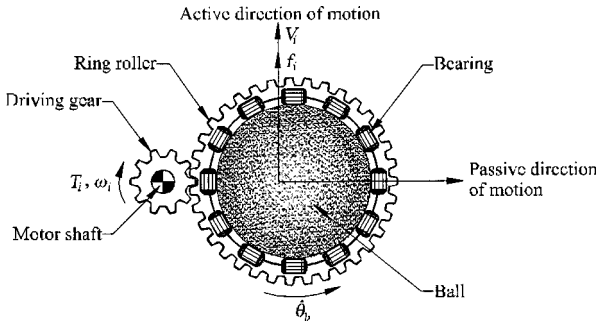


**Fig. 5 Free body diagram of actuator-ball coupling**

Finally, by substituting for the left-hand side of Eq. (16) by Eq. (12) and Eq. (15) while adding the passive friction forces given by Eq. (11), one obtains

$$k_f \begin{bmatrix} -s & -s & s & s \\ c & -c & -c & c \\ L & L & L & L \\ L & -L & L & -L \end{bmatrix} \begin{bmatrix} u_1 \\ u_2 \\ u_3 \\ u_4 \end{bmatrix} = \begin{bmatrix} M_v+s^2M_m & 0 & 0 & 0 \\ 0 & M_v+c^2M_m & 0 & 0 \\ 0 & 0 & I_A+I_B+I_C+L^2M_m & I_A-I_B \\ 0 & 0 & I_A-I_B & I_A+I_B+L^2M_m \end{bmatrix} \begin{bmatrix} \dot{V}_{vx} \\ \dot{V}_{vy} \\ \ddot{\phi}_v \\ \ddot{\phi} \end{bmatrix} + \begin{bmatrix} D_x+s^2D_m+scM_m\dot{\Phi} & 0 & 0 & 0 \\ 0 & D_y+c^2D_m-scM_m\dot{\Phi} & 0 & 0 \\ 0 & 0 & D_{\Phi_v}+L^2D_m & 0 \\ 0 & 0 & 0 & D_{\phi}+L^2D_m \end{bmatrix} \begin{bmatrix} V_{vx} \\ V_{vy} \\ \dot{\phi}_v \\ \dot{\phi} \end{bmatrix} + \begin{bmatrix} \cos(\phi_v) \\ -\sin(\phi_v) \\ 0 \\ 0 \end{bmatrix} \sin(\theta) M_v g + \begin{bmatrix} c & -c & -c & c \\ s & s & -s & -s \\ 0 & 0 & 0 & 0 \\ 0 & 0 & 0 & 0 \end{bmatrix} \times \begin{bmatrix} \mathrm{sgn}(v_{ap}) & 0 & 0 & 0 \\ 0 & \mathrm{sgn}(v_{bp}) & 0 & 0 \\ 0 & 0 & \mathrm{sgn}(v_{cp}) & 0 \\ 0 & 0 & 0 & \mathrm{sgn}(v_{dp}) \end{bmatrix} \begin{bmatrix} f_{ap} \\ f_{bp} \\ f_{cp} \\ f_{dp} \end{bmatrix} + k_t \begin{bmatrix} -s & -s & s & s \\ c & -c & -c & c \\ L & L & L & L \\ L & -L & L & -L \end{bmatrix} \times \begin{bmatrix} \mathrm{sgn}(v_a) & 0 & 0 & 0 \\ 0 & \mathrm{sgn}(v_b) & 0 & 0 \\ 0 & 0 & \mathrm{sgn}(v_c) & 0 \\ 0 & 0 & 0 & \mathrm{sgn}(v_d) \end{bmatrix} \begin{bmatrix} f_{ta} \\ f_{tb} \\ f_{tc} \\ f_{td} \end{bmatrix} \tag{17}$$

where $k_f = 2\rho k/R$ is the motor voltage-force conversion factor, $M_m = 16\rho^2 I_m/R^2$ is the dynamic effect of the motor inertias on the mass vehicle, $D_m = 16\rho^2 d_m/R^2$ is the dynamic effect of the motor damping on the translational damping of the vehicle, $k_t = 1/(\sin(\alpha)R) = 2/R$ is the ball torque-force conversion factor. Notice that Eq. (4) and Eq. (6) are used to obtain the individual ball's active and passive velocities. For obtaining this model, it was necessary to differentiate the Jacobian matrix leading to nonlinear Coriolis terms in the damping matrix.

## 4 Transmission Analysis and Optimization

As will be shown in this section, the novel CVT design of the vehicle demonstrates interesting features regarding power trans-

mission and power consumption. Here, the performance and optimization issues of power transmission are considered in detail. It is shown how to select a suitable base angle to maximize the speed or the acceleration in a desired direction. Moreover, the relation between power losses due to friction and base angle is studied.

**4.1 Maximum Vehicle Speed.** The dynamic model presented in the previous section and given by Eq. (17) is derived for the case when current-regulating motor drivers are used. These are responsible for keeping the current supplied to the motors, within certain limits, proportional to a desired value irrespective of the rotational speed or the loading conditions. Thus, back electromotive forces (emf) do not appear in the mentioned dynamics model. However, and for power analysis purposes, we will neglect these drivers in this section and include the back electromotive forces. This, of course, will influence only the left hand side of Eq. (17) which corresponds to the generalized force vector generated by the motors to overcome the inertia, damping, and friction forces of the vehicle (Fig. 6).

A simplified armature circuit is considered to model the dynamics of the used DC-motors. The inductance of the armature is neglected, as its corresponding time constant is much smaller than the mechanical time constant. The voltage supplied to motor $i$ is given by

$$u_i(t) = R_m i(t) + k_m \omega_i , \tag{18}$$

where $R_m$, $i$, $k_m$, $\omega_i$, and $k_m\omega_i$ are the armature resistance, current, motor torque constant, motor speed, and the back emf respectively. Accordingly, the torque $Ti$ generated by motor $i$ is

$$T_i(t) = k_m(u_i(t) - k_m \omega i)/R_m . \tag{19}$$

Following the previous derivation steps, the generalized force vector generated by the motors is found to be

$$\begin{bmatrix} F_x \\ F_y \\ M_{\phi_v} \\ M_\phi \end{bmatrix} = K_f \begin{bmatrix} -s & -s & s & s \\ c & -c & -c & c \\ L & L & L & L \\ L & -L & L & -L \end{bmatrix} \begin{bmatrix} u_1 \\ u_2 \\ u_3 \\ u_4 \end{bmatrix} - K_e \begin{bmatrix} s^2 & 0 & 0 & 0 \\ 0 & c^2 & 0 & 0 \\ 0 & 0 & L^2 & 0 \\ 0 & 0 & 0 & L^2 \end{bmatrix} \begin{bmatrix} V_{vx} \\ V_{vy} \\ \dot{\phi}_v \\ \dot{\phi} \end{bmatrix}, \tag{20}$$

which can replace the left-hand side of Eq. (17). Here, $K_f = 2\rho k_m/(R_m R) = 42.0\,[\mathrm{N/V}]$ is the motor voltage-force conversion factor, $K_e = 16\rho^2 k_m^2/(R_m R^2) = 4730\,[\mathrm{N\cdot s/m}]$ corresponds to the back electromotive forces. Now, assuming that loads on all balls are equal, then for steady-state motion on the horizontal plane, Eq. (17) becomes

$$K_f \begin{bmatrix} -s & -s & s & s \\ c & -c & -c & c \\ L & L & L & L \\ L & -L & L & -L \end{bmatrix} \begin{bmatrix} u_1 \\ u_2 \\ u_3 \\ u_4 \end{bmatrix} = \begin{bmatrix} 4cf_p + 4sk_t f_t & 0 & 0 & 0 \\ 0 & 4sf_p + 4ck_t f_t & 0 & 0 \\ 0 & 0 & 4Lk_t f_t & 0 \\ 0 & 0 & 0 & 4Lk_t f_t \end{bmatrix} \begin{bmatrix} sign(V_{vx}) \\ sign(V_{vy}) \\ sign(\dot{\phi}_v) \\ sign(\dot{\phi}) \end{bmatrix}$$

$$+ \begin{bmatrix} K_e s^2 + D_x + s^2 D_m + scM_m\dot{\Phi} & 0 & 0 & 0 \\ 0 & K_e c^2 + D_y + c^2 D_m - scM_m\dot{\Phi} & 0 & 0 \\ 0 & 0 & K_e L^2 + D_{\Phi_v} + L^2 D_m & 0 \\ 0 & 0 & 0 & K_e L^2 + D_\phi + L^2 D_m \end{bmatrix} \begin{bmatrix} V_{vx} \\ V_{vy} \\ \dot{\phi}_v \\ \dot{\phi} \end{bmatrix} \tag{21}$$

Thus, for a simple motion in the positive x-direction, the steady-state vehicle velocity becomes

$$V_{vx} = 4\,\frac{sK_f u - (cf_p + sk_t f_t)}{K_e s^2 + D_x + s^2 D_m} = 4\,\frac{s(K_f u - k_t f_t) - cf_p}{s^2(K_e + D_m) + D_x}, \tag{22}$$

where

$$u = -u_1 = -u_2 = u_3 = u_4 . \tag{23}$$

Figure 7 shows the vehicle velocity as a function of the base angle. Hence, for maximizing the velocity for the given parameters and for $u = 24\,[\mathrm{volt}]$, one should choose the base angle to be around 7 degrees. However, the base angle is physically limited to values higher than 27.5 degrees, then the best solution should be around this limit. It is worth noting that the optimal base angle depends on the mechanical gear ratio, which is fixed to be 8; changing this gear ratio yields different velocity-base angle relations and thus it becomes possible to achieve maximum velocity even within the limits of the base angle.

**4.2 Maximum Acceleration: Impedance Matching.** For a traditional servomotor coupled to its mechanical load via a reduction gear, a suitable gear ratio can be selected to maximize the power transmitted to the load (to maximize the acceleration for example) for a given voltage. In other words, the impedances of the motor and the load are matched [6]. For our CVT vehicle, this can be achieved by selecting (through the mechanical design) the gear ratio between the motors and the balls, and by selecting a suitable base angle.

For maximizing the acceleration of the vehicle in the

**Fig. 6 Prototype of the wheelchair**

$x$-direction, for example, let us examine Eq. (17). Increasing the base angle (as seen from the left-hand side) increases the force transmitted to the vehicle, from the right-hand side decreasing this angle decreases the effective vehicle mass. Thus, there is an optimum value for the base angle that produces the maximum acceleration. Figure 8 shows the acceleration of the vehicle in the $x$-direction for different speeds and base angles given a constant voltage input $u=24\,[\text{volt}]$. It is noticed that increasing the base angle leads to increasing the negative slope of the acceleration-velocity curve. There is a critical speed (about 0.6 m/s in Fig. 8) before which increasing the base angle increases the acceleration whereas after this critical angle the opposite happens. Let assume a zero velocity, then the acceleration is

$$\dot{V}_{vx}=\frac{-4sK_f u}{M_v+s^2M_m}, \tag{24}$$

which has a maximum at

$$M_v=s^2M_m, \tag{25}$$

recalling that $M_v=87\,[\text{kg}]$ and $M_m=50.6\,[\text{kg}]$, it becomes clear that increasing the base angle increases the acceleration. The optimum value cannot be achieved, for the given parameters, by changing only the base angle since $s^2<1$. However, as $\rho$ is imbedded in both $K_f$ and $M_m$, one can select a gear ratio $\rho$ greater than 8 to produce optimality. In other words, as the impedance matching depends on both the hard gear ratio $\rho$ and on the soft gear ratio $\phi$, optimality is achieved by selecting suitable values for the two.

As the vehicle is supposed to move in any direction in the $x$-$y$ plane, achieving impedance matching calls for choosing an appropriate value for the base angle depending on the desired motion. Let us assume that

$$\begin{aligned}\ddot{\phi}_v&=\ddot{\phi}=0,\\ \dot{V}_{vy}&=\gamma\dot{V}_{vx},\end{aligned} \tag{26}$$

i.e., the vehicle's acceleration has only $x$- and $y$-components. Then, from Eq. (17), the first two constraints yield

$$\begin{aligned}u_3&=-u_1,\\ u_4&=-u_2,\end{aligned} \tag{27}$$

while the third constraint implies that

$$u_2=\frac{c(M_v+s^2M)+\gamma s(M_v+c^2M)}{c(M_v+s^2M)-\gamma s(M_v+c^2M)}u_1, \tag{28}$$

accordingly,

$$\dot{V}_{vx}=\frac{-4scK_f}{c(M_v+s^2M)-\gamma s(M_v+c^2M)}u_1, \tag{29}$$

Thus the maximum vehicle acceleration occurs when

$$(c^3+\gamma s^3)M_v=s^2c^2(c+\gamma s)M_m, \tag{30}$$

which reduces to the same expression for the special case ($\gamma=0$). Notice that the selection of an appropriate base angle depends not only on the masses of the vehicle and the motors but also on the direction of motion $\gamma$. Accordingly, one can achieve impedance matching and thus maximum acceleration dynamically by changing the base angle $\phi$.

**4.3 Power Efficiency.** To maximize the power efficiency of the vehicle, the power losses through friction and twisting torque should be minimized. This can be achieved by selecting suitable materials for the balls without affecting the traction properties. Moreover, it is possible to minimize power losses by selecting a suitable base angle as the friction forces and twisting torques depend explicitly on it.

From Eq. (17), the power losses through in friction and twisting $P_{lost}$, while assuming equally distributed loads on the wheels, is

$$P_{lost}=\begin{bmatrix}4cf_p+4sk_tf_t & 0 & 0 & 0\\ 0 & 4sf_p+4ck_tf_t & 0 & 0\\ 0 & 0 & 4Lk_tf_t & 0\\ 0 & 0 & 0 & 4Lk_tf_t\end{bmatrix}\times\begin{bmatrix}sign(V_{vx})\\ sign(V_{vy})\\ sign(\dot{\phi}_v)\\ sign(\dot{\phi})\end{bmatrix}[V_{vx}\;\;V_{vy}\;\;\dot{\phi}_v\;\;\dot{\phi}] \tag{31}$$

Notice that the base angle appears only in translational motion terms. Accordingly, let us assume a general plane motion with

$$\begin{aligned}V_{vx}&=\cos(\delta)V_v\\ V_{vy}&=\sin(\delta)V_v\end{aligned} \tag{32}$$

where $\delta$ denotes the direction of motion. Hence, the power losses become

$$P_{los}=(\cos(\delta)*(4cf_p+4sk_tf_t)+\sin(\delta)*(4sf_p+4ck_tf_t))V_v. \tag{33}$$

Figure 9 shows the power losses, for different values of $\delta$, as a function of the base angle. Thus, to minimize the power losses

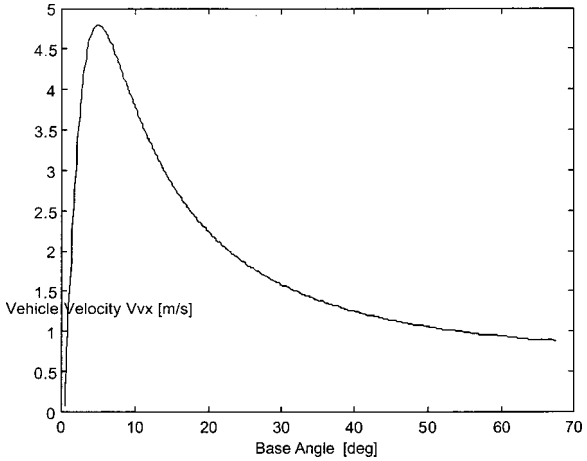


**Fig. 7 Vehicle velocity versus base angle**

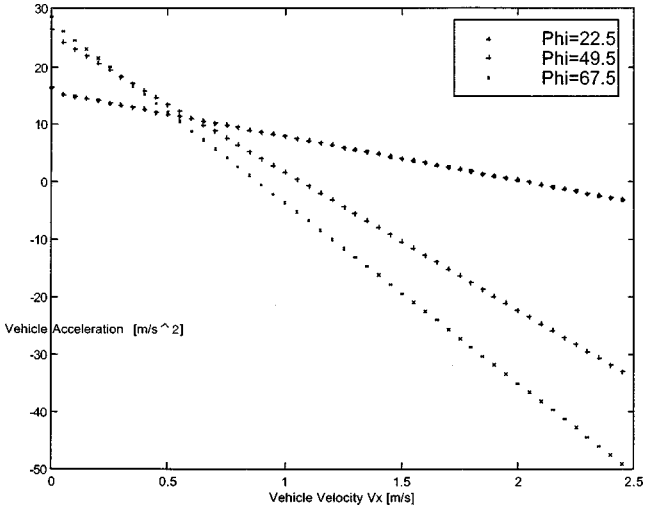


**Fig. 8 Vehicle acceleration versus velocity**

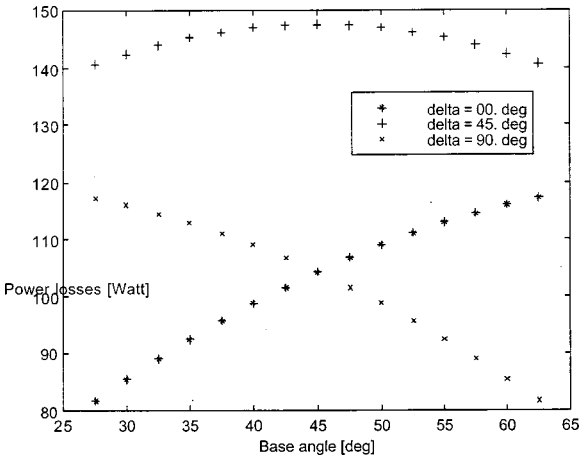


**Fig. 9 Power losses as function of base angle and direction of motion**

**Table 1 Identified prototype parameters**

| Parameter | Value | Unit |
|---|---|---|
| $k_f$ | 40.25 | $N/volt$ |
| $k_t$ | 37.0 | $1/m$ |
| $L$ | 0.35 | $m$ |
| $M_v$ | 87.0 | $Kg$ |
| $M_m$ | 50.6 | $Kg$ |
| $D_m$ | 22.8 | $N.sec/m$ |
| $D_x = D_y$ | 28.4 | $N.sec/m$ |
| $D_{\Phi v}$ | 12.3 | $N.m.sec/rad$ |
| $D_\Phi$ | 40.9 | $N.m.sec/rad$ |
| $I_A = I_B$ | 1.12 | $Kg.m^2$ |
| $I_C$ | 3.62 | $Kg.m^2$ |
| $f_{ip}$ | 8.0 | $N$ |
| $f_{ti}$ | 0.78 | $N.m$ |

through friction, a small base angle in the direction of motion should be selected. Moreover, it is not recommended to move with both $x$ and $y$ velocity components as friction forces will add up. As before, friction forces and twisting torques and thus power losses depend on the hard gear ratio as well as on the soft gear ratio. For optimality both of these two variables should be selected carefully.

In conclusion, an interesting scheduling problem arises. Based on the planned motion trajectory, an optimal base angle can always be selected to assure maximum acceleration (at the beginning e.g.,) maximum steady-state velocity, or minimum power loss. This can be achieved either manually or automatically by means of the above-derived equations.

As a matter of fact and to the knowledge of the authors, this is the first multi-degree-of-freedom CVT design. Here, the gear ratio can be defined as the relationship between four motor velocities and the two velocity components.

## 5 Control

The vehicle's model, derived in Eq. (17), reflects a nonlinear and time-varying dynamics. The inertia and damping matrices contain terms that change with the configuration. Moreover, Coriolis forces may appear if it is desired to change the footprint configuration while the vehicle is moving. In contrast to all of these terms, which are ''theoretically'' easy to model and estimate, there exist always substantial friction forces that dominate the dynamics in steady motions. These friction forces not only depend on the loads on the individual balls and the terrain characteristics but they depend also on the base angle. This leads to the exclusion of feedback linearization control techniques from being applied to this system. Accordingly, one may consider an adaptive control scheme that relies on robust parameter estimation.

However it is desired to design a simple robust controller that can be implemented in real time using available onboard hardware. Thus, we would like to consider a PD controller. Fortunately, the vehicle's four degrees of freedom are mainly decoupled as can be seen from the right-hand side of Eq. (17). Hence, it is possible to design a decoupled SISO controller for each degree of freedom and then to find the necessary control input (motor voltages) using the left-hand side of the equation. In general, the PD controller looks like

$$u = -k_p(x - x_d) - k_v\dot{x}, \tag{32a}$$

where $k_p$ and $k_v$ are the proportional and derivative feedback gains, $x_d$ and $x$ are the desired and measured positions. The performance of this control law degrades in the presence of friction and can result in substantial tracking and steady-state errors. It can be shown that in order to minimize the steady-state error, the proportional feedback gain must be increased which leads to a more sensitive and to a less robust performance. To avoid this problem, the estimated resultant friction force $\hat{F}$ acting on a specific degree of freedom can be fed forward as

$$u = -k_p(x - x_d) - k_v\dot{x} + \hat{F}. \tag{33a}$$

Depending on the accuracy of the estimated friction force, the performance will be very close to a system without friction. Thus, the problem of friction compensation necessitates accurate estimation of the friction force. Amin [7] suggested a method for estimating Coulomb-like friction based on a nonlinear observer. Assuming a dynamic model of the form

$$\ddot{x} = w - F(\dot{x}), \tag{34}$$

where $w$ is the force (acceleration assuming unit mass) due to all sources other than friction force $F(\dot{x})$. The observer is defined then by

$$\begin{aligned} \hat{a} &= z - k_{obs}|\dot{x}|^{\mu_{obs}} \\ \hat{F} &= \hat{a}\, sign(\dot{x}), \end{aligned} \tag{35}$$

where $k_{obs}$ and $\mu_{obs}$ are design parameters, $a$ is the magnitude of the friction force, and the variable $z$ is given by

$$\dot{z} = k_{obs}\mu_{obs}|\dot{x}|^{\mu_{obs}-1}[w - \hat{F}]sign(\dot{x}) \tag{36}$$

It is shown in [7] that the estimation error converges asymptotically to zero by choosing $k_{obs} > 0$ and $\mu_{obs} > 0$. However, the design lacks a method to determine suitable values for the two parameters.

## 6 Simulation Experiments

**6.1 Parameter Identification.** As an application example, a chair is mounted on the vehicle to form a robotic wheelchair. The parameters of the prototype shown in Fig. 6 corresponding to the model given in Eq. (17) are identified. For this purpose a set of experiments are designed where the frequency and time responses to various inputs are examined. The results of identification are summarized in Table 1.

All experiments were performed for the wheelchair with no user while using rubber balls on a PVC ground. Moreover, it is assumed that loads on all balls are equal. Logically, the user's weight should be included within the mass of the vehicle. Both passive friction force and twisting torque vary with the weight of the vehicle; experiments with three different weights show that in average

$$f_{ti} = 0.33 + 0.007M_v\,, \tag{37}$$

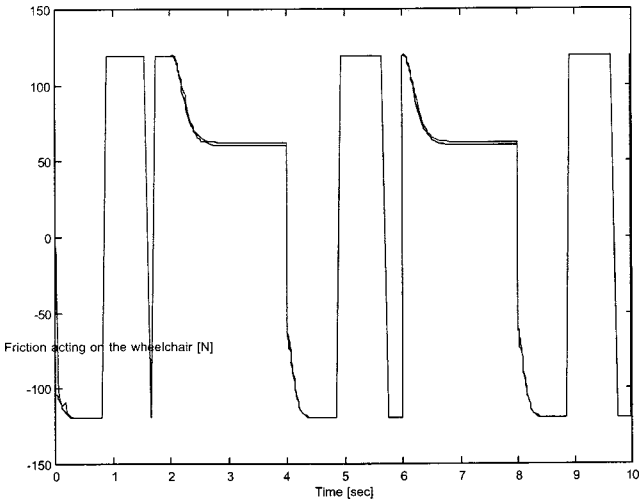


**Fig. 10 Estimated and actual friction force for y-motion**

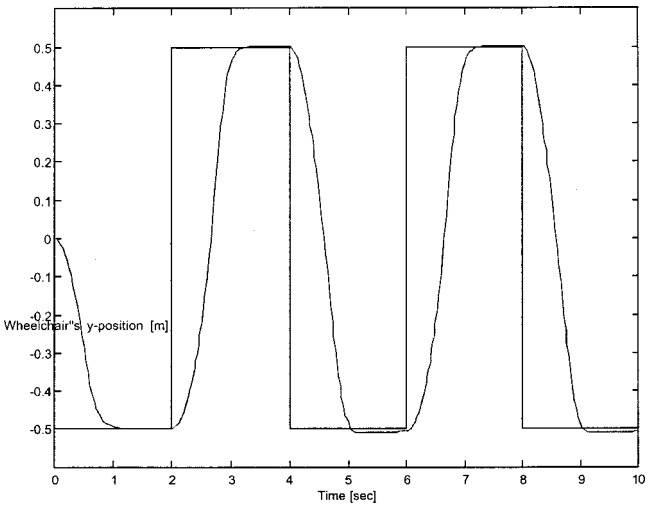


**Fig. 12 Desired and actual vehicle's position along the y-axis with motor saturation**

$$f_{ip} = 0.13 M_v ,$$

where the constant term in the twisting torque is contributed mainly by the internal friction of the motor and the gear. This yields the approximate coefficients of friction (see Eq. (10))

$$\mu_p = 4^* f_{ip} / (M_v g) = 0.053. \tag{38}$$

**6.2 Implementation and Simulation.** To show the applicability of the control method, a simulation environment under SIMULINK is developed. The full model as given by Eq. (17) is defined as the plant. The vehicle is commanded to follow square waves corresponding to the four degrees of freedom.

The proportional and derivative feedback gains of the controller are selected to generate a closed-loop system with a natural frequency $\omega_n = 10$ rad/s and a damping ratio $\zeta = 1$. As expected, the PD-controller performs well in terms of transient response but it can not achieve a zero steady-state error without increasing the proportional gain to very high values.

Accordingly, the observer of the last section is used to estimate the friction forces. Although the friction forces are not always constant, the observer is able to estimate them very well after tuning the observer parameters ($k_{obs} = 3000$, $\mu_{obs} = 2$). Figure 10 shows the actual and estimated friction force acting on the vehicle's y-translational DOF; this DOF is selected for illustration as the last two DOFs exhibit constant friction forces. With this, it becomes possible to compensate for the friction; Fig. 11 shows the tracking error for the third DOF where the steady-state error vanishes.

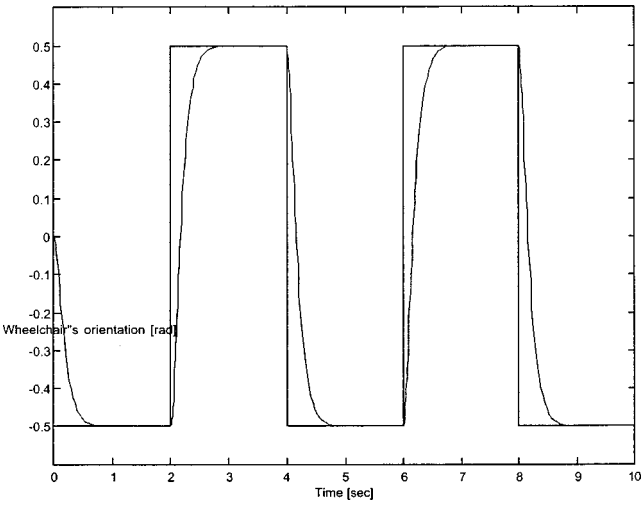


**Fig. 11 Desired and actual vehicle's orientation angle with friction compensation**

The estimation of friction depends on the full knowledge of the inertia and damping matrices. This assumption is hard to meet in reality as the uncertainty in parameters knowledge is high. Thus it is more reasonable to try to estimate the friction given only a rough model of the system. Hence, in the following, only a constant approximation of the inertia and damping matrices elements were given to the observer. Simulation results show that the estimation error is reasonable everywhere except when the beams angle $\phi$ switches direction. Then, the approximate model becomes rough due to the very big Coriolis terms. However, one can still use this estimate to compensate for friction. Then, it can be seen that the steady-state error is still close to zero for all degrees of freedom.

Finally, the effect of motor saturation is studied. Figure 12 shows the tracking errors for one of the vehicle's motions after introducing a saturation element in the simulation corresponding to $u_i = 10$ volt while the observer has only an approximate model. This figure shows that, even with the approximate observer model and motor saturation, the performance of the PD-controller with friction compensation is acceptable.

## 7 Conclusions

In this paper, a novel design of an omnidirectional vehicle is presented. Kinematic and dynamic models of this ball-based footprint configurable CVT vehicle are derived. Friction and twisting torque effects are discussed and included. The advantages gained by the CVT feature are analyzed and discussed. Finally, a simple PD-controller with friction compensation is considered and simulation results show its applicability.

Friction forces vary depending not only on the load and terrain characteristics but on the base angle as well. This makes the friction characteristics highly complex and difficult to model. To overcome this difficulty an adaptive friction compensation technique is applied to the system.

## Nomenclature

$D_m$ = motors damping projected on vehicle damping, Kg/s

$D_x$ = vehicle damping coefficient in the $x$-direction, kg/s

$\mathbf{F_i}$ = ball traction forces vector, N
$\mathbf{F_v}$ = vehicle generalized forces vector, N, N·m
$F$ = actual friction force, N
$\hat{F}$ = estimated friction force, N
$I_A$, $I_B$, and $I_C$ = inertia of beam A, beam B, and vehicle, Kg·m·m
$I_m$ = motor and ball combined inertia, Kg·m·m
$J$ = Jacobian: balls active velocities $\mathbf{V_i}$ to vehicle generalized velocities $\mathbf{V_v}$,
$K_e$ = back electromotive force lumped constant, Kg/s
$K_f$ = motor voltage-force conversion factor, N/volt
L = distance between the pivotal joint to the ball-contact point with the ground, m
$M_m$ = motors inertia projected on vehicle mass, Kg
$M_v$ = vehicle mass, Kg
$P$ = Jacobian: generalized vehicle velocities $\mathbf{V}_v$ to balls passive velocities $\mathbf{V}_{ip}$,
$P_{los}$ = power losses in friction and twisting, Watt
$R$ = ball radius, m
$R_m$ = motor resistance, Ohm
$Ti$ = torque generated by motor $i$, N·m
$Tw_i$ = twisting torque of ball $i$, N·m
$V_i$ = ball i active velocity, m/s
$V_{ip}$ = ball i passive velocity, m/s
$V_{ix}$ = $x$ component of ball $i$ active velocity, m/s
$V_{iy}$ = $y$ component of ball $i$ active velocity, m/s
$V_{vx}$ = $x$ component of vehicle velocity, m/s
$V_{vy}$ = $y$ component of vehicle velocity, m/s
$W_i$ = weight of vehicle acting on ball $i$, N
$a$ = friction force magnitude in observer model, N
$d_m$ = motor and ball combined damping, Kg·m/s
$f_{ip}$ = Coulomb friction force acting on ball $i$, N
$f_{ti}$ = twisting torque magnitude of ball $i$, N·m
$i$ = current supplied to motor, Amp
$k$ = motor constant, N·m/Volt
$k_f$ = motor voltage-force conversion factor, N/volt
$k_{obs}$ and $\mu_{obs}$ = observer design parameters,
$k_p$ = proportional feedback gain, N/m
$k_m$ = back electromotive force constant, volt·s
$k_v$ = derivative feedback gain, N·sm
$k_t$ = ball torque-force conversion factor, l/m
$x$ = measured position, m
$x_d$ = desired position, m
$u_i$ = voltage input to motor $i$, Volt
$w$ = non-friction forces, N
$z$ = friction observer state, N
$\alpha$ = inclination angle of the ring, degree
$\phi$ = base angle: half of the angle between the beams, degree
$\phi_v$ = vehicle orientation: angle between the bisector of the beams and a stationary Cartesian $x$-axis, degree
$\mu_p$ = Coulomb coefficient of friction
$\rho$ = gear reduction ratio
$\theta$ = vehicle inclination angle from the horizontal, degree
$\omega_A$, $\omega_B$, $\omega_C$ = Angular velocity of beam A, beam B, and vehicle, rad/s
$\omega_i$ = angular velocity of motor $i$, rad/s

## References


[1] Gott, P., 1991, "Changing Gears: The Development of the Automatic Transmission," SAE, Inc., pp. 25–30.
[2] Guzzella, L., and Schmid, A., 1995, "Feedback Linearization of Spark-Ignition Engines with Continuously Variable Transmissions," IEEE Trans. Control Syst., **3**, No. 1, pp. 54–60.
[3] Hirose, S., Tibbetts, C., and Hagiwara, T., 1999, "Development of X-Screw: A Load-Sensitive Actuator Incorporating a Variable Transmission," IEEE International Conference on Robotics and Automation, pp. 193–199.
[4] Pin, F., and Killough, M., 1994, "A New Family of Omnidirectional and Holonomic Wheeled Platform for Mobile Robots," IEEE Trans. Rob. Autom., **10**, No. 4, pp. 480–489.
[5] Wada, M., and Asada, H., 2000, "Design and Control of a Variable Footprint Mechanism for Holonomic Omnidirectional Vehicles and Its Application to Wheelchair," IEEE Trans. Rob. Autom., **16**, No. 1, pp. 1–9.
[6] Auslander, D., 1996, *Mechatronics: Mechanical System Interfacing*, Prentice Hall, NJ.
[7] Amin, J., Friedland, B., and Harony, A., 1997, "Implementation of a Friction Estimation and Compensation Technique," IEEE Control Syst. Mag., **17**, No. 4, pp. 71–76.